

# A First Estimate Of The X-Ray Binary Frequency As A Function Of Star Cluster Mass In A Single Galactic System

D. M. Clark <sup>1,2</sup>, S. S. Eikenberry <sup>2</sup>, B. R. Brandl <sup>3</sup>, J. C. Wilson <sup>6</sup>, J. C. Carson <sup>5</sup>, C. P. Henderson <sup>4</sup>, T. L. Hayward <sup>7</sup>, D. J. Barry <sup>4</sup>, A. F. Ptak <sup>8</sup>, E. J. M. Colbert <sup>8</sup>

## ABSTRACT

We use the previously-identified 15 infrared star-cluster counterparts to X-ray point sources in the interacting galaxies NGC 4038/4039 (the Antennae) to study the relationship between total cluster mass and X-ray binary number. This significant population of X-Ray/IR associations allows us to perform, for the first time, a statistical study of X-ray point sources and their environments. We define a quantity,  $\eta$ , relating the fraction of X-ray sources per unit mass as a function of cluster mass in the Antennae. We compute cluster mass by fitting spectral evolutionary models to  $K_s$  luminosity. Considering that this method depends on cluster age, we use four different age distributions to explore the effects of cluster age on the value of  $\eta$  and find it varies by less than a factor of four. We find a mean value of  $\eta$  for these different distributions of  $\eta = 1.7 \times 10^{-8} M_{\odot}^{-1}$  with  $\sigma_{\eta} = 1.2 \times 10^{-8} M_{\odot}^{-1}$ . Performing a  $\chi^2$  test, we demonstrate  $\eta$  could exhibit a positive slope, but that it depends on the assumed distribution in cluster ages. While the estimated uncertainties in  $\eta$  are factors of a few, we believe this is the first estimate made of this quantity to “order of magnitude” accuracy. We also compare our findings to theoretical models of open and globular cluster evolution, incorporating the X-ray binary fraction per cluster.

---

<sup>1</sup>Instituto de Astronomía, Universidad Nacional Autónoma de México, Apdo Postal 877, Ensenada, Baja California, México; dmclark@astrosen.unam.mx

<sup>2</sup>Department of Astronomy, University of Florida, Gainesville, FL 32611; dmclark@astro.ufl.edu

<sup>3</sup>Leiden University, P.O. Box 9513, 2300 RA Leiden, Netherlands.

<sup>4</sup>Astronomy Department, Cornell University, Ithaca, NY 14853.

<sup>5</sup>Max Planck Institute for Astronomy, Königstuhl 17, D-69117 Heidelberg, Germany

<sup>6</sup>Department of Astronomy, P.O Box 400325, University of Virginia, Charlottesville, VA 22904.

<sup>7</sup>Gemini Observatory, AURA/Casilla 603, La Serena, Chile

<sup>8</sup>Department of Physics and Astronomy, Johns Hopkins University, 3400 North Charles St., Baltimore, MD 21218.

*Subject headings:* galaxies: starburst – galaxies: star clusters – X-rays: binaries

## 1. Introduction

The Antennae are a pair of colliding galaxies with an unusually large number of X-ray point sources. High resolution X-ray observations taken with *Chandra* revealed 49 new individual sources (Fabbiano, Zezas, & Murray 2001), where previous observations only indicated extended filamentary structure (Fabbiano et al. 1997). These X-ray sources range in luminosity from  $10^{38} - 10^{40}$  ergs s $^{-1}$ . Most of these are thought to be X-ray binaries (XRBs) with a black hole compact companion (Fabbiano, Zezas, & Murray 2001).

In addition to numerous X-ray sources, the Antennae contain many bright, massive young clusters that are evident in both optical, *HST* (Whitmore et al. 1999) and infrared (IR) (Brandl et al. 2005, henceforth Paper I) images. This makes this pair of interacting galaxies an ideal target for studying the environments of XRBs. In Clark et al. (2007, henceforth Paper II) we performed an extensive study of the XRB environments using *Chandra* X-ray images and *J* and *K<sub>s</sub>* IR images (Paper I). Our present paper will expand on our previous study by exploring the relationship between XRBs and cluster mass in the Antennae.

Recent theoretical models of young, massive cluster evolution provide a framework for comparison to our observational study. Two in particular, (Oskinova 2005; Sepinsky, Kalogera, & Belczynski 2005), incorporate the fraction of XRBs per cluster in their models. Oskinova (2005) use a population synthesis code to study the evolution of X-ray emission in young, massive clusters. Sepinsky, Kalogera, & Belczynski (2005) investigate the role of supernova kicks in XRB expulsion from the parent cluster using the population synthesis code, StarTrack. They also incorporate the number of XRBs for a range in cluster mass. We will compare our measurements of the fraction of XRBs per cluster in the Antennae to those predicted by these models.

We organize our paper as follows: In §2 we give a brief summary of our previous work on the Antennae and then define a quantity,  $\eta$ , relating the XRB fraction to cluster mass in the Antennae. In our analysis, we estimate cluster mass using *K<sub>s</sub>* luminosity, which depends non-trivially on the assumed cluster age. We explore cluster age/luminosity relations and their impact on our mass estimates in §3. We compare  $\eta$  to the measured value predicted by theoretical cluster evolutionary models and present conclusions in §4.

## 2. Observations and Data Analysis

### 2.1. Infrared Images

This paper is based on infrared (IR)  $J$  ( $1.25\ \mu\text{m}$ ) and  $K_s$  ( $2.15\ \mu\text{m}$ ) images of the Antennae galaxies. We initially presented these data and discussed the details of their reduction in Paper I. In summary, 20-minute total exposures in each filter were acquired using the Wide-field InfraRed Camera (WIRC – see Wilson et al. (2003) for details) on the Palomar 5-m telescope during the night of March 22nd, 2002. In Paper II, we made a frame-tie between the IR and X-ray images using IR counterparts to circumvent the poor absolute astrometric accuracy of *Chandra* ( $\sim 1''.5$ ). We matched seven IR sources from the WIRC images with *Chandra* X-ray point sources. Using a least squares fit of a linear matching function we tied *Chandra* right ascension and declination to WIRC  $x$ ,  $y$  pixel positions. The rms positional uncertainty is  $\sim 0''.5$ . With a strong astrometric frame-tie in place we were able to accurately identify IR counterparts to X-ray sources. We found 19 IR counterparts within  $1''.5$  of an X-ray source, 13 of which were within  $1''.0$  of an X-ray source. After estimating the IR source density, we predict only two of the “strong” matches (separations  $< 1''.0$ ) and three of the “possible” matches (separations between  $1''.0 - 1''.5$ ) are due to chance superpositions of unrelated objects.

In Paper II, we pointed out two important implications for these results. First, that there is clearly a significant excess of IR counterparts within  $1''.0$  of the X-ray sources – 13, where we expect only two in the null hypothesis of no physical counterparts. Even including the “possible” counterparts out to  $1''.5$ , we have a total of 19 counterparts, where we expect only five are chance superpositions. Secondly, this implies that for any given “strong” IR counterpart, we have a probability of  $\sim 85\%$  ( $11/13$  with a  $1\sigma$  uncertainty of  $0.3^1$ ) that the association with an X-ray source is real. Even for the “possible” counterparts, the probability of true association is  $\sim 50\%$ . Therefore, regardless of the physical separations between the X-ray sources and their IR counterpart, we are confident that the majority of these associations are real.

We note that of the 19 X-ray sources with counterparts, two are the nuclei (Zezas et al. 2002a), one is a background quasar (Clark et al. 2005), and two share the same IR counterpart. Therefore, in this paper we will only consider the 15 IR counterparts (of the original 19) that are star clusters in the Antennae.

---

<sup>1</sup>Found using confidence levels for small number statistics listed in Tables 1 and 2 of Gehrels (1986).

## 2.2. Photometry

We performed aperture photometry in both the  $J$  and  $K_s$  bands on all 15 IR cluster counterparts plus an additional 204 clusters identified by eye in these IR images of the Antennae (see also Paper I and the tables there-in). We defined our aperture as  $\sim 3\sigma$  of the Gaussian PSF, where  $J$  had a full width at half maximum (FWHM) of  $1''.2$  and  $K_s$  had a FWHM of  $0''.9$ . We measured a mean and median sky background flux in two separate annuli between  $\sim 6 - 10\sigma$  of the PSF. To account for the exceptionally crowded field of the Antennae, we employed the use of background arcs instead of annuli. Multiplying these four measurements by the area of the central aperture and then subtracting these from the flux in the central aperture yielded four separate source flux measurements. We defined error in sky background,  $\sigma_{sky}$ , as the standard deviation of the four measured source fluxes. We also considered Poisson noise,  $\sigma_{adu}$ , defined as the total source flux divided by the square root of the gain for the WIRC instrument. The gain for WIRC during the observations was  $2e^-DN^{-1}$  (Wilson et al. 2003)<sup>2</sup>. Adding  $\sigma_{sky}$  and  $\sigma_{adu}$  in quadrature, we computed the total error in flux,  $\sigma_{flux}$ . We converted fluxes to magnitudes using a bright, 2MASS star in the field and defined the error in magnitude,  $\sigma_m$ , as  $\sigma_{flux}$  divided by the mean flux. Typical errors in magnitude were  $\sim 0.06$  mag in both bands, with no error above 1.0 mag.

To estimate cluster masses we needed to compute  $K_s$  luminosity ( $M_{K_s}$ ). We computed  $M_{K_s}$  using reddening derived from  $(J - K_s)$  colors (Paper II). Assuming all clusters are dominated by O and B stars, their intrinsic  $(J - K_s)$  colors are  $\sim 0.2$  mag. Approximating this value as 0 mag, this allowed us to estimate  $A_{K_s}$  as  $\simeq (J - K_s)_{obs}/1.33$  using the extinction law defined in Cardelli, Clayton, & Mathis (1989).

## 2.3. XRB-to-Cluster Mass Fraction

We assume for now that cluster mass is proportional to  $K_s$  luminosity – i.e. that the stellar composition of all clusters is the same. We defined a luminosity cutoff for statistical purposes as  $M_{K_s} = -13.2$  mag (see Paper II for details). We binned the data by 0.2 mag in  $M_{K_s}$  and then calculated an average flux per bin. Computing the fraction of the total number of clusters per average flux of each bin, we took this as the probability of finding a cluster with a specific mass. In Figure 1 we compare this probability for both clusters with X-ray sources and all clusters in the Antennae. This shows that XRBs are more common in

---

<sup>2</sup>At the time of the Antennae observations, WIRC was equipped with a Hawaii-1 1K×1K detector and this is the gain for it.

more massive clusters.

This result is not surprising – as star cluster mass increases, so does the number of massive stars in it. Through stellar evolution, a certain fraction of these stars will die in supernova explosions, leaving behind neutron star or black hole remnants. In turn, a fraction of these stellar remnants will retain/acquire a mass-donating companion star, becoming a detectable XRB. Thus, through sheer numbers of stars in more massive clusters, we expect a greater likelihood of finding XRBs in them. This leads us to two interesting questions: 1) quantitatively, what cluster mass will more likely produce an XRB and 2) is there some intrinsic property of massive cluster physics that favors the production of XRBs, beyond simple scaling with mass?

We believe that our large sample of IR-to-X-ray associations provides the first dataset sufficient to estimate the answers to these questions for the Antennae galaxies. In our approach to answer these questions we explore the relationship between the number of X-ray detections per unit mass as a function of cluster mass in the Antennae. We can formalize this expression in the following equation:

$$N_X(M_c) = N_{Cl}(M_c) \cdot \eta(M_c) \cdot M_c \quad (1)$$

Here,  $N_X(M_c)$  is the number of detected X-ray sources with an IR cluster counterpart,  $N_{Cl}(M_c)$  is the number of detected clusters, and  $\eta(M_c)$  is the fraction of X-ray sources per unit mass, all as a function of cluster mass,  $M_c$ .

If  $\eta(M_c)$  increases or decreases over a range in  $M_c$ , this means there could be something peculiar about massive cluster physics to favor or suppress XRB formation. In contrast, a constant  $\eta(M_c)$  across all  $M_c$  would indicate that more massive clusters are more likely to have an XRB simply because they have more stars.

While  $\eta(M_c)$  is a powerful tool in studying the number of XRBs per cluster, it requires that we know the mass of each star cluster. However, extrapolating the masses of the Antennae clusters from our photometric data required models that called for estimates of ages and metallicities. While we successfully constrained these inputs and determined cluster masses (see below and §3), we first sought to compute  $\eta(M_c)$  in terms of a purely observable quantity – flux. Calculating  $\eta(M_c)$  as a function of  $K_s$ -band flux,  $\eta(F_{K_s})$ , allowed us to investigate non-model dependent trends in  $\eta(M_c)$ .

We calculated  $\eta(F_{K_s})$  for clusters with a  $K_s$ -band luminosity brighter than the -13.2 mag cutoff using bin sizes of  $F_{K_s} = 4 \times 10^6$  in counts (DN) (Figure 2). This bin size was small enough to show a trend in  $\eta(F_{K_s})$ , but large enough to contain at least two clusters

with X-ray sources, allowing us to assign error bars to each value of  $\eta(F_{K_s})$ . The errors plotted on the graph are the measurement uncertainty in the mean value of the four  $\eta(F_{K_s})$  added in quadrature with the Poisson uncertainty of the mean  $\eta(F_{K_s})$  in each bin. Due to the small sample size per bin, we computed these uncertainties using the small number statistics formulae described in Keeping (1962). Figure 2 shows that  $\eta(F_{K_s})$  is roughly consistent with a constant value of  $5.4 \times 10^{-8} F_{K_s}^{-1}$  with an uncertainty of  $\sigma_{\bar{\eta}} = 1.8 \times 10^{-8} F_{K_s}^{-1}$ .

In essence,  $\eta(F_{K_s})$  is comparing two different mass distributions,  $N_{Cl}(F_{K_s})$ , the mass distribution for all clusters in the Antennae and  $N_X(F_{K_s})/F_{K_s}$ , the mass distribution for clusters with X-ray sources, normalized by flux. If there is a constant number of X-ray sources per unit cluster mass as suggested by Figure 2, then these two mass distributions should be the same. We can further corroborate this result by comparing  $N_X(F_{K_s})/F_{K_s}$  and  $N_{Cl}(F_{K_s})$  using a two-sided Kolmogorov-Smirnov (K-S) test. The K-S test yielded a D-statistic of 0.75 and a probability of 0.107 that they are related. Considering the separate cluster mass populations as two probability distributions, each can be expressed as a cumulative distribution. The D-statistic is then the absolute value of the maximum difference between each cumulative distribution. This test quantitatively demonstrates that there is nothing peculiar about massive clusters in the Antennae with associated XRBs. We also computed the Pearson  $r$  linear correlation coefficient between  $N_X(F_{K_s})/F_{K_s}$  and  $N_{Cl}(F_{K_s})$ , finding a value of 0.99. Since a value of 1 means a perfect linear fit, this value of  $r$  further substantiates the observed relationship in  $\eta(F_{K_s})$ .

We then converted  $\eta(F_{K_s})$  into the more conventional units of solar mass. Here we assume all clusters are coeval. Selecting  $M_{K_s}$  listed in the Bruzual-Charlot (BC) cluster evolutionary models (Bruzual & Charlot 2003) for a 20 Myr,  $1M_{\odot}$  cluster as a typical value in the Antennae (Whitmore et al. 1999), we converted the model  $M_{K_s}$  to  $F_{K_s}$  using the standard relationship between luminosity and flux. Multiplying  $\eta(F_{K_s})$  by  $F_{K_s}$  we converted  $\eta(F_{K_s})$  to solar masses: assuming a cluster metallicity of  $z = 0.02$ ,  $\eta = 5.8 \times 10^{-8} M_{\odot}^{-1}$  with an uncertainty of  $\sigma_{\bar{\eta}} = 1.9 \times 10^{-8} M_{\odot}^{-1}$ , while assuming a metallicity of  $z = 0.05$ ,  $\eta = 8.9 \times 10^{-8} M_{\odot}^{-1}$  with an uncertainty of  $\sigma_{\bar{\eta}} = 3.0 \times 10^{-8} M_{\odot}^{-1}$ .

While we assume all clusters are  $\sim 20$  Myr old, we note that the actual range in ages should be  $\sim 1$ – $100$  Myr (Whitmore et al. 1999). The BC models indicate that clusters in this age range could vary by a factor of as much as 100 in mass for a given  $K_s$  luminosity. Since  $\eta$  is a function of mass, incorrectly assigning cluster ages has the potential to significantly impact  $\eta$ . In the next section, we explore how differences in cluster age can affect the value of  $\eta$ .

### 3. Effects of Age and Slope in $\eta$

We investigated the effect differences in cluster age has on  $\eta$  by assuming three individual age distributions for the Antennae clusters: an instant burst in which all clusters are the same age, a uniform distribution, and a distribution of the form,  $dN/d\tau \propto \tau^{-1}$  (Fall, Chandar, & Whitmore 2005). In each case, we assumed all clusters have solar metallicity ( $z = 0.02$ ) (Whitmore et al. 1999).

In addition, we address the issue of whether the functional form of  $\eta(M_c)$  can be fit by a slope or if, indeed,  $\eta(M_c)$  is consistent with a single value, by performing a  $\chi^2$  test. We computed the  $\Sigma\chi^2$  between the  $\eta$  values for each bin and the mean value of  $\eta$ , and computed the  $\Sigma\chi^2$  between the  $\eta$  values for each bin and a fitted line to these values. The difference between the two value of  $\Sigma\chi^2$ ,  $\Delta\Sigma\chi^2$ , indicated the significance of the fitted slope. If  $\Delta\Sigma\chi^2$  was less than one, with in one  $\Sigma\chi^2$  deviation, then this indicated that the fitted slope was insignificant. While a value of  $\Delta\Sigma\chi^2$  between one and two, with in two  $\Sigma\chi^2$  deviations, indicated only a weak slope. Any value of  $\Delta\Sigma\chi^2$  greater than two meant a significant, nonzero slope in  $\eta$ . For our initial case, where we estimated cluster mass using  $F_{K_s}$  we found  $\Delta\Sigma\chi^2 = 1.9$ , suggesting a weak, but non-negligible slope, in  $\eta$ .

Considering the case of an instant burst in star formation, we assigned the same age to describe all clusters and picked several such values in the range 1 – 100 Myr. Applying the BC models, we converted  $\eta(F_{K_s})$  to units of solar mass for a range in ages. For each distribution in  $\eta$  we computed a mean value (Figure 3). The mean for these values is  $\eta_{instant} = 3.3 \times 10^{-8} M_{\odot}^{-1}$  with a standard deviation of  $\sigma_{instant} = 2.9 \times 10^{-8} M_{\odot}^{-1}$ .

Performing our  $\chi^2$  test for each distribution in  $\eta$  (see Figure 3), we found a mean in  $\Delta\Sigma\chi^2$  of 0.86, with a standard deviation,  $\sigma_{\Delta\Sigma\chi^2} = 1.7$ . This seems to indicated conflicting results. For some cases in assumed cluster age there is no significant slope in  $\eta$ , while other cases show a pronounced slope. This becomes more evident by examining Figure 3, which shows a range in  $\Delta\Sigma\chi^2$  of  $\sim 0$ –6.5. Incidentally, for  $\eta_{20}$ ,  $\Delta\Sigma\chi^2 = 2.2$ , while for  $\eta_{100}$ ,  $\Delta\Sigma\chi^2 = 4.8 \times 10^{-3}$ .

Next, we assumed a uniform age distribution for our Antennae cluster sample. Picking ages at random from a uniform distribution between 1 – 100 Myr, we assigned an age to each cluster in our sample. Applying the BC models, we computed each cluster’s mass based on the assigned age, produced a mass distribution, and then calculated a mean  $\eta$ . Performing a Monte Carlo (MC) simulation, we recreated cluster mass distributions 10,000 times, producing a large sample of  $\eta$ ’s with a mean of  $\bar{\eta}_{uniform} = 5.4 \times 10^{-9} M_{\odot}^{-1}$  and  $\sigma_{\bar{\eta}_{uniform}} = 6.3 \times 10^{-10} M_{\odot}^{-1}$  (Figure 4).

We then administered our  $\chi^2$  test for each realized distribution of  $\eta$ , finding a mean

$\overline{\Delta\Sigma}\chi^2 = 5.9$  and  $\sigma_{\overline{\Delta\Sigma}\chi^2} = 5.2$ . In some cases,  $\eta$  didn't exhibit a positive slope. Therefore, we investigated whether the slope in  $\eta$  tended to be mostly positive or mostly negative by multiplying each  $\overline{\Delta\Sigma}\chi^2$  statistic by the sign of the slope. In doing so, we found a mean  $\overline{\Delta\Sigma}\chi^2 = 5.8$  and  $\sigma_{\overline{\Delta\Sigma}\chi^2} = 5.3$ . Thus almost all distributions in  $\eta$  for the uniform case had a positive slope.

A more realistic approach is assuming the cluster ages are defined by a power law (PL):  $dN/d\tau \propto \tau^{-1}$  (Fall, Chandar, & Whitmore 2005). These authors derived their relationship using *HST* *UBVIH $\alpha$*  observations of  $\sim 11,000$  clusters. Fitting BC models to photometry of each cluster, they generated an age distribution. In our analysis we picked ages at random according to this distribution. Mirroring the procedure used for the uniform distribution case above, we created a sample of 10,000  $\eta$  values. We found a mean for this sample of  $\overline{\eta}_{PL} = 8.7 \times 10^{-9} M_{\odot}^{-1}$  and a  $\sigma_{\overline{\eta}_{PL}} = 1.2 \times 10^{-9} M_{\odot}^{-1}$ .

Performing our  $\chi^2$  test as we did with the uniform age distribution case, we found a mean  $\overline{\Delta\Sigma}\chi^2 = 5.1$  and  $\sigma_{\overline{\Delta\Sigma}\chi^2} = 6.0$ . Accounting for variations in the sign of the slope in  $\eta$ , we found  $\overline{\Delta\Sigma}\chi^2 = 4.3$  and  $\sigma_{\overline{\Delta\Sigma}\chi^2} = 6.6$ . Therefore, the trend in the slope of  $\eta$  remains positive, but not as significantly as the uniform age distribution case.

In a final scenario, we used the cluster ages listed in the electronic table available through Mengel (2005) to fit ages to 144 clusters in our sample, including all 15 clusters associated with X-ray sources. Mengel (2005) derived ages by using three age indicators – *UBVI* and *K $_s$*  broadband photometry to break the age/reddening degeneracy, *H $\alpha$*  and *Br $\gamma$*  emission to identify clusters less than 7 Myr, and CO band-head absorption from narrow-band images for clusters  $\sim 10$  Myr. They then fit these data to theoretical spectra for ages  $< 500$  Myr using a  $\chi^2$  minimization technique (for details, see Mengel 2005).

Following the method discussed in §2.3, we used the BC models to convert  $M_{K_s}$  to mass for those clusters with Mengel (2005) age estimates. Using cluster bins of  $1.0 \times 10^7 M_{\odot}$  in mass, we computed four values for  $\eta$  (see Figure 5). The errors plotted on the graph are uncertainties in the mean value of  $\eta$  added in quadrature with the Poisson uncertainty in each bin. Again, we used the small number statistic formulae in Keeping (1962) to compute these errors. We found a mean in  $\eta$  of  $2.2 \times 10^{-8} M_{\odot}^{-1}$  and  $\sigma_{\overline{\eta}} = 1.2 \times 10^{-8} M_{\odot}^{-1}$ . Applying our  $\chi^2$  test, we found  $\Delta\Sigma\chi^2 = 1.0 \times 10^{-2}$ , implying no significant slope in  $\eta$ .

We summarize our age analysis in Figure 6. Comparing the distributions in  $\eta$  for the fitted ages, instant burst, uniform and power law age distributions, all values for  $\eta$  are within a factor of four. Assuming an instant burst of 20 Myr,  $\eta$  differs by a factor of ten (see Figure 6). Excluding specific ages for instant bursts of cluster formation, there is little variation in the value of  $\eta$ .



Comparing our  $\chi^2$  test for each of the four different age assumptions indicates inconsistent results (see Table 1). In the instant burst, uniform and power law cases, the slope in  $\eta$  varies from insignificant to distinctly positive, while  $\eta$  has no significant slope when the ages derived by Mengel (2005) are fit to our clusters. Therefore, we can not ignore that  $\eta$  might have a non-zero slope and we will discuss the implications of this in the following section.

#### 4. Summary and Conclusions

Through the quantity  $\eta$ , our investigation revealed conflicting results with respect to the relationship between observed number of XRBs and cluster mass. We performed a  $\chi^2$  test on the slope in  $\eta$  for a variety of assumed star cluster age distributions and found some cases where the slope was insignificant, while other cases showed a distinctly positive slope. No slope indicates the observed number of XRBs per unit mass is independent of cluster mass, while a positive slope in  $\eta$  suggests more XRBs per unit mass are produced in more massive clusters. In the following discussion, we will consider both a constant value in  $\eta$  as well as a slope in  $\eta$ , and the implications of each result.

Initially, we estimated cluster mass by fitting BC spectrophotometric models to cluster  $M_{K_s}$ , assuming all clusters are  $\sim 20$  Myr. Recognizing that this method depends on cluster age, we explored how different assumptions of a cluster age distribution for the Antennae affect  $\eta$  and showed that  $\eta$  varies by a factor of roughly four; although including individual ages for the instant bursts case will increase the variations in  $\eta$  to a factor of 10.

We now proceed by comparing the mean value of  $\eta$  for the four different assumed age distributions,  $\eta = 1.7 \times 10^{-8} M_{\odot}^{-1}$ , to that predicted by models of young, massive clusters. We will compare  $\eta$  to theoretical models discussed in Oskinova (2005) and Sepinsky, Kalogera, & Belczynski (2005).

In a recent study presented in Oskinova (2005), the author modeled X-ray emission from young, massive star clusters, assuming a closed system with constant mass, no dynamics and all stars are coeval, with cluster metallicities of either  $z = 0.02$  or  $z = 0.008$ . These models predict  $\sim 2\text{--}5\%$  of all OB stars in a cluster should produce high mass X-ray binaries (HMXBs). In the models in Oskinova (2005), all clusters are assumed to have masses of  $M_{cl} = 10^6 M_{\odot}$  with stellar masses ranging from  $1 - 100 M_{\odot}$ . Considering the Salpeter initial mass function (IMF) of the form  $\xi(M) = M_0 M^{-2.35}$  and defining stars with masses  $> 8 M_{\odot}$  as “OB stars”, for our purposes here, we estimated  $6\%$  of all stars in the model clusters are OB stars. Therefore,  $1 - 3 \times 10^{-3}$  of all stars in a cluster with an initial mass of  $3 \times 10^6 M_{\odot}$  (set by the Salpeter IMF) should produce an XRB. Since the Salpeter IMF implies there are  $7 \times 10^5$

stars in a cluster, then these stars should produce  $7 - 22 \times 10^2$  XRBs – orders of magnitude greater than the  $\sim 49$  observed in the Antennae. Expressing  $\eta$  as a fraction of XRBs-to-cluster mass, the models in Oskinova (2005) suggest  $\eta$  ranges from  $3 - 7 \times 10^{-4} M_{\odot}^{-1}$ . These values are greater by at least a factor of 1000 from our estimates for  $\eta$ . Clearly, this predicts a much larger number of compact object binaries than what we observed in the Antennae. Oskinova (2005) note that they were unable to detect HMXBs in three massive ( $\sim 10^4 M_{\odot}$ ) clusters which they predict should contain between 1-3 HMXBs. If our measured value for  $\eta$  accurately describes the number of HMXBs formed, then it is not surprising that Oskinova (2005) fail to find any. As pointed out by these authors, future modeling of HMXB formation is needed to understand the discrepancy between the predictions and observations of XRB populations in starburst galaxies.

In another study, Sepinsky, Kalogera, & Belczynski (2005) use the binary evolution and population synthesis code, StarTrack (Belczynski et al. 2002), to investigate the rate of XRB formation and ejection from young, massive clusters. This program tracks stellar parameters such as radius, luminosity, mass and core mass. The simulations are stopped at the formation of a compact object. The models include mass transfer in binaries and include transient XRBs. Sepinsky, Kalogera, & Belczynski (2005) consider cluster masses ranging from  $5 \times 10^4 M_{\odot}$  to  $5 \times 10^6 M_{\odot}$  and cluster ages from 1 to  $\sim 20$  Myr and compute the average number of XRBs within 1–1000 pc of the cluster center.

Considering the typical cluster age in the Antennae is 20 Myr, Sepinsky, Kalogera, & Belczynski (2005) predict a  $5 \times 10^4 M_{\odot}$  cluster should contain 0.13 XRBs, while 15 XRBs should reside in a  $5 \times 10^6 M_{\odot}$  cluster. Here we assume that an XRB is associated with a cluster if it is within 100 pc. This separation is equivalent to  $1''.0$  at the distance of the Antennae (for  $H_0 = 75 \text{ km s}^{-1} \text{ Mpc}^{-1}$ ), which is our criteria for an XRB-cluster association (Paper II). These model predictions for XRB detections assume a limiting X-ray luminosity of  $L_X = 5 \times 10^{35} \text{ ergs s}^{-1}$ , but the observed limiting luminosity in the Antennae is  $2 \times 10^{37} \text{ ergs s}^{-1}$ . Using the X-ray luminosity function (XLF) for the Antennae defined in Zezas & Fabbiano (2002), we scaled the XRB results of Sepinsky, Kalogera, & Belczynski (2005) to estimate what these models would predict for the observed number of XRBs in the Antennae clusters. Using a XLF power law slope of  $\alpha = -0.45$  (Zezas & Fabbiano 2002), the models predict 0.02 XRBs are observed in a  $5 \times 10^4 M_{\odot}$  cluster, while 2.7 XRBs should be seen in a  $5 \times 10^6 M_{\odot}$  cluster, at the luminosity limits of the X-ray observations. Expressing these model results as a fraction of XRBs-to-cluster mass, we can directly compare them to our measured value for  $\eta$  in the Antennae. Doing so, Sepinsky, Kalogera, & Belczynski (2005) predict  $\eta$  ranges from  $4 - 5 \times 10^{-7} M_{\odot}^{-1}$ , with in a factor of five from our predictions for  $\eta$ . As mentioned by Sepinsky, Kalogera, & Belczynski (2005), several caveats exist for their models including: 1) assumed binary fraction of unity which could lead to over estimates of the mean number of

XRBs per cluster, 2) the stellar, power-law IMF can affect the XRB fraction per cluster, and 3) changes in the half-mass radius can strongly influence the median XRB distance from the cluster. These factors could potentially explain the discrepancies between their models and our observations.

Since some forms of  $\eta$  exhibit a distinctly positive slope, these models may not always apply to  $\eta$ . More importantly, a positive slope has implications for star formation scenarios in clusters. As mentioned above, a positive slope implies more XRBs per unit mass are produced in more massive clusters. If an abnormally large number of XRBs exist in a star cluster, then the progenitors of their compact objects should also possess an over abundance. Since the progenitors are massive stars, this implies star formation in massive clusters favors stars at the heavier end in mass. This is not unusual. Work by Stolte et al. (2005) suggest some of the largest clusters in the Milky Way could have a top heavy mass function.

In this paper we introduced the quantity,  $\eta$ , relating the fraction of X-ray sources per unit mass as a function of cluster mass. Applying this function to the Antennae, we revealed several important environmental implications for the X-ray sources in the Antennae. Specifically,  $\eta$  predicts a far different relationship between XRB formation and cluster mass than that predicted by Oskinova (2005) and is broadly consistent with that predicted by Sepinsky, Kalogera, & Belczynski (2005). Clearly, future cluster modeling with particular emphasis on the relationship between the number of XRBs in a galaxy and the galactic cluster environment is essential to explain our current observations. Furthermore, a  $\chi^2$  test demonstrated the functional form of  $\eta$  did not always remain consistent with a single value, but for some assumptions for a cluster age distributions, the slope had a significantly positive value. While this could imply a top heavy mass function in massive clusters, our statistics are small. We plan to enlarge our statistical base by extending our observational study to additional starburst galaxies. We can then address whether the properties of  $\eta$  depend on an individual galaxy or are consistent across all galactic environments.

The authors thank the staff of Palomar Observatory for their excellent assistance in commissioning WIRC and obtaining these data. WIRC was made possible by support from the NSF (nsf-ast0328522), the Norris Foundation, and Cornell University. S.S.E. and D.M.C. are supported in part by an NSF CAREER award (NSF-9983830). We also thank J.R. Houck for his support of the WIRC instrument project. The authors are also grateful for many long and insightful discussions with M.L. Edwards.

## REFERENCES

- Anders, P., de Grijs, R., Fritze-v. Alvensleben, U., & Bissantz, N. 2004, MNRAS, 347, 17
- Belczynski, K., Kalogera, V., & Bulik, T. 2002, ApJ, 572, 407
- Brandl, B.R., et al. 2005, ApJ, 635, 280
- Bruzual, G. & Charlot, S. 2003, MNRAS, 344, 1000
- Cardelli, J.A., Clayton, G.C., & Mathis, J.S. 1989, ApJ, 345, 245
- Clark, D.M., et al. 2005, ApJ, 631, L109
- Clark, D. M., et al. 2007, ApJ, 658, 319
- Fabbiano, G. 1995, in X-Ray Binaries, ed. W.H.G. Lewin, J. van Paradijs, & E.P.J. van den Heuvel (Cambridge: Cambridge Univ. Press), 390
- Fabbiano, G., Schweizer, F., & Mackie, G. 1997, ApJ, 478, 542
- Fabbiano, G., Zezas, A., & Murray, S.S. 2001, ApJ, 554, 1035
- Fall, S.M. 2006, ApJ, in press
- Fall, S.M., Chandar, R., & Whitmore, B.C. 2005, 631, L133
- Gehrels, N. 1986, ApJ, 303, 336
- Harris, W.E. 1996, AJ, 112, 1487
- Keeping, E.S. 1962, Introduction To Statistical Inference, (Princeton; van Nostrano), p.202
- Mengel, S., Lehnert, M.D., Thatte, N., & Genzel, R. 2005, Å, 443, 41
- Oskinova, L.M. 2005, MNRAS, 361, 679
- Pooley, D., et al. 2003, ApJ, 591, L131
- Portegies Zwart, S.F., Hut, P., McMillan, S.L.W., & Makino, J. 2004, MNRAS, 351, 473
- Sepinsky, J., Kalogera, V., & Belczynski, K. 2005, ApJ, 621, L37
- Stolte, A., Brandner, W., Grebel, E.K., Lenzen, R., & Lagrange, A. 2005, ApJ, 628, L113.
- Wilson, J.C., et al. 2003, Proc. SPIE, 4841, 451

- Zezas, A., Fabbiano, G., Rots, A.H., & Murray, S.S. 2002, ApJ, 142, 239
- Zezas, A., Fabbiano, G., Rots, A.H., & Murray, S.S. 2002, ApJ, 577, 710
- Zezas, A., & Fabbiano, G. 2002, ApJ, 577, 726
- Whitmore, B.C., Zhang, Q., Leitherer, C., & Fall, S.M. 1999, AJ, 118, 1551

Table 1.  $\Delta\Sigma\chi^2$  Statistics

Age Test	$\Delta\Sigma\chi^2$	$\sigma_{\Delta\Sigma\chi^2}$	Median $\Delta\Sigma\chi^2$
flux	1.9	—	—
20 Myr	2.2	—	—
100 Myr	$4.8\times 10^{-3}$	—	—
Mengle	$1.0\times 10^{-2}$	—	—
Instant	0.86	1.7	0.10
Uniform	5.9	5.2	4.7
Uniform <sup>1</sup>	5.8	5.3	4.7
Power Law	5.1	6.0	2.8
Power Law <sup>1</sup>	4.3	6.6	2.1

Note. — For instant, uniform and power law cases,  $\Delta\Sigma\chi^2$  statistics are mean values.

<sup>1</sup>Multiplied  $\Delta\Sigma\chi^2$  by the sign of the slope for the fitted line.

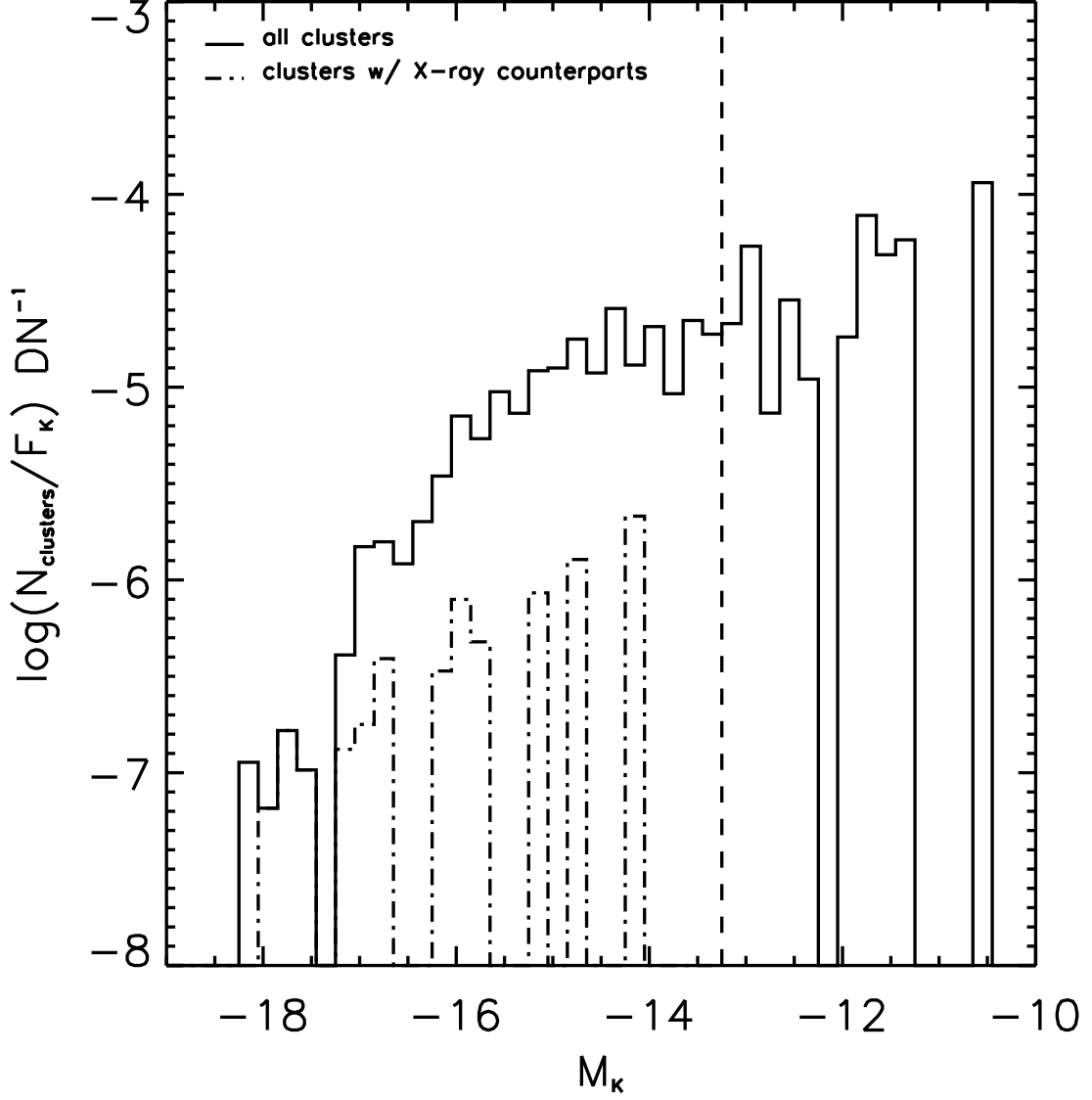


Fig. 1.— Here we plot  $M_{K_s}$  versus the number of clusters in each bin divided by mean flux in that bin. Each bin is 0.2 mag. Arguing that mass is proportional to flux, this graph shows the probability of finding a cluster with a given mass. The dashed line signifies the magnitude cutoff,  $M_{K_s} = -13.3$  mag.

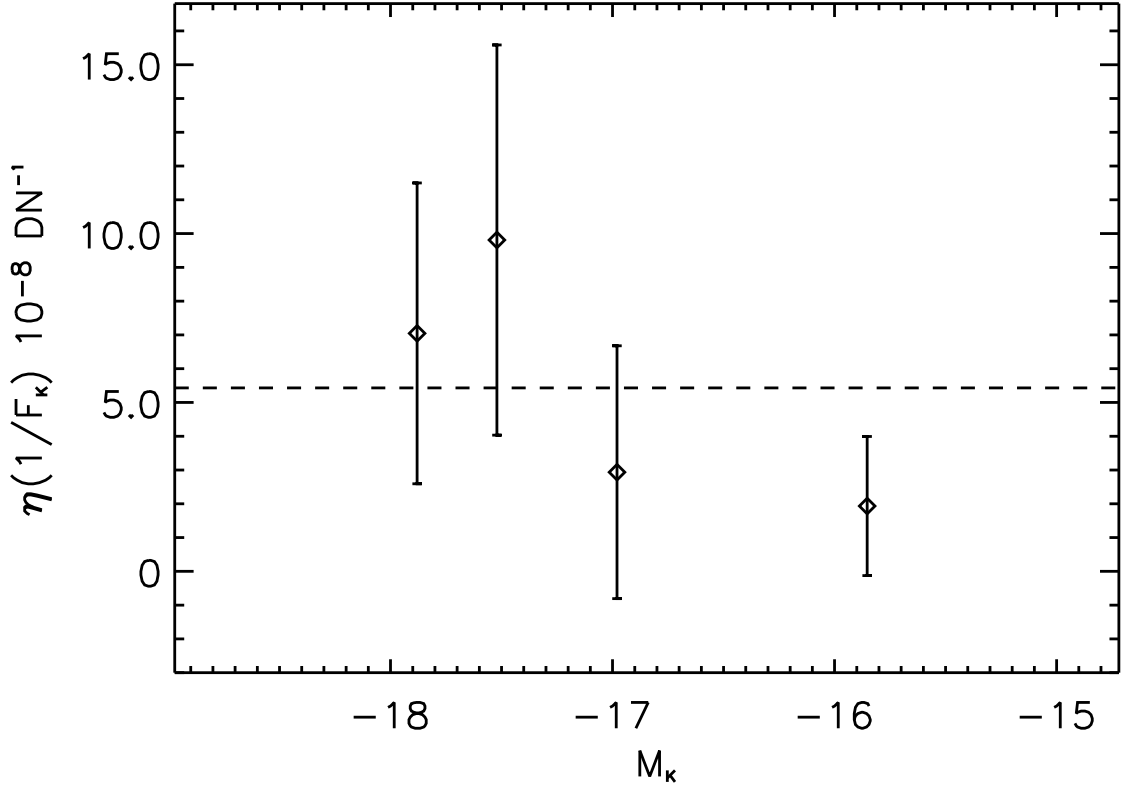


Fig. 2.— This figure displays  $\eta(F_{K_s})$  plotted versus  $M_{K_s}$ . The bins are  $F_{K_s} = 4 \times 10^6 \text{ DN}^{-1}$  in size. Error bars are the uncertainties in the mean value of  $\eta$  added in quadrature with the Poisson uncertainty in each bin. The dotted line is the mean of the four  $\eta(F_{K_s})$  values.



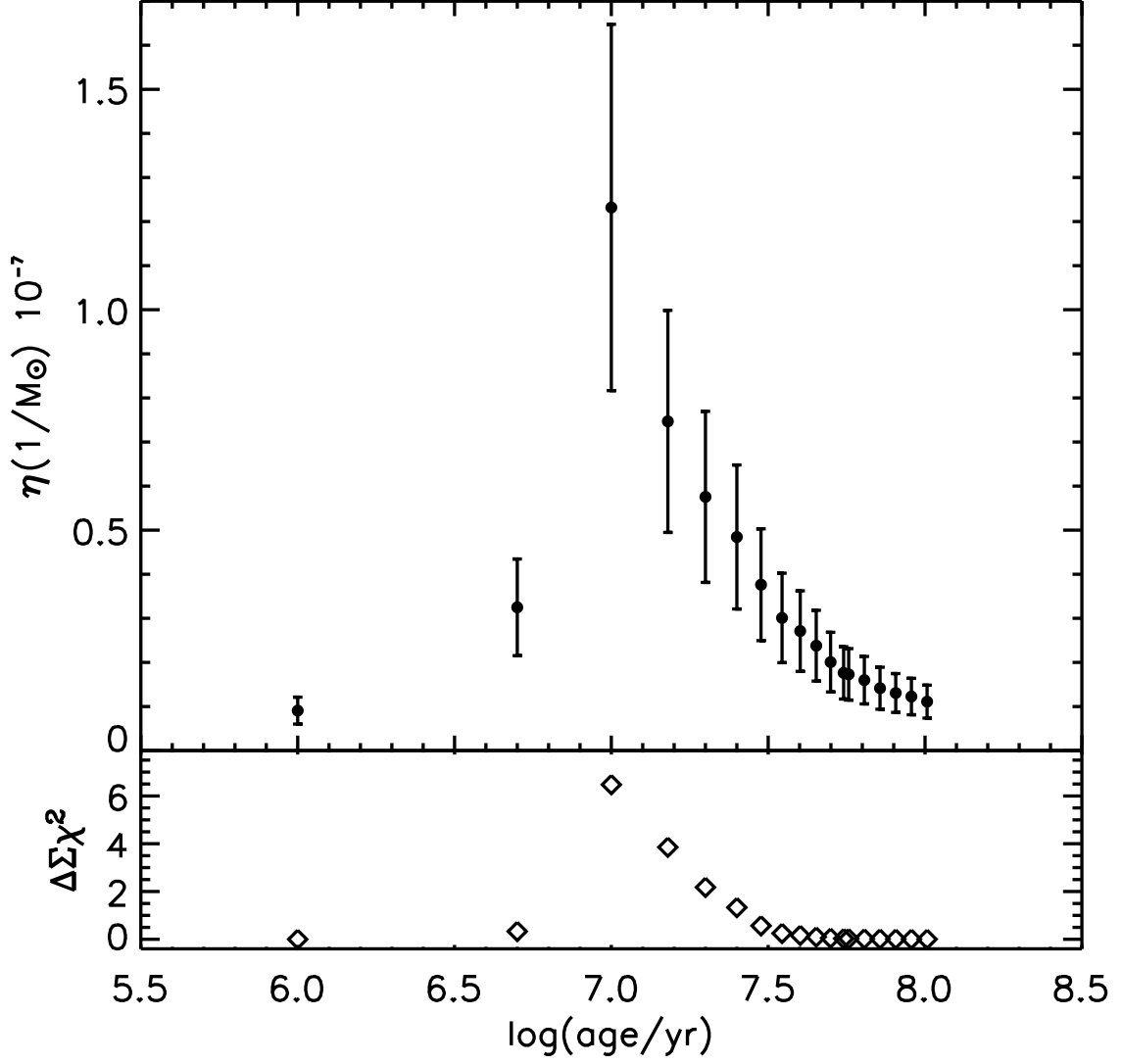


Fig. 3.— Assuming an instant burst of star formation in the Antennae, we plot the mean value of  $\eta$  for a range in ages between 1 - 100 Myr. Notice the factor of  $\sim 10$  range in  $\eta$  as well as the degeneracy in  $\eta$  in this age range. Error bars are uncertainties in  $\eta$ .

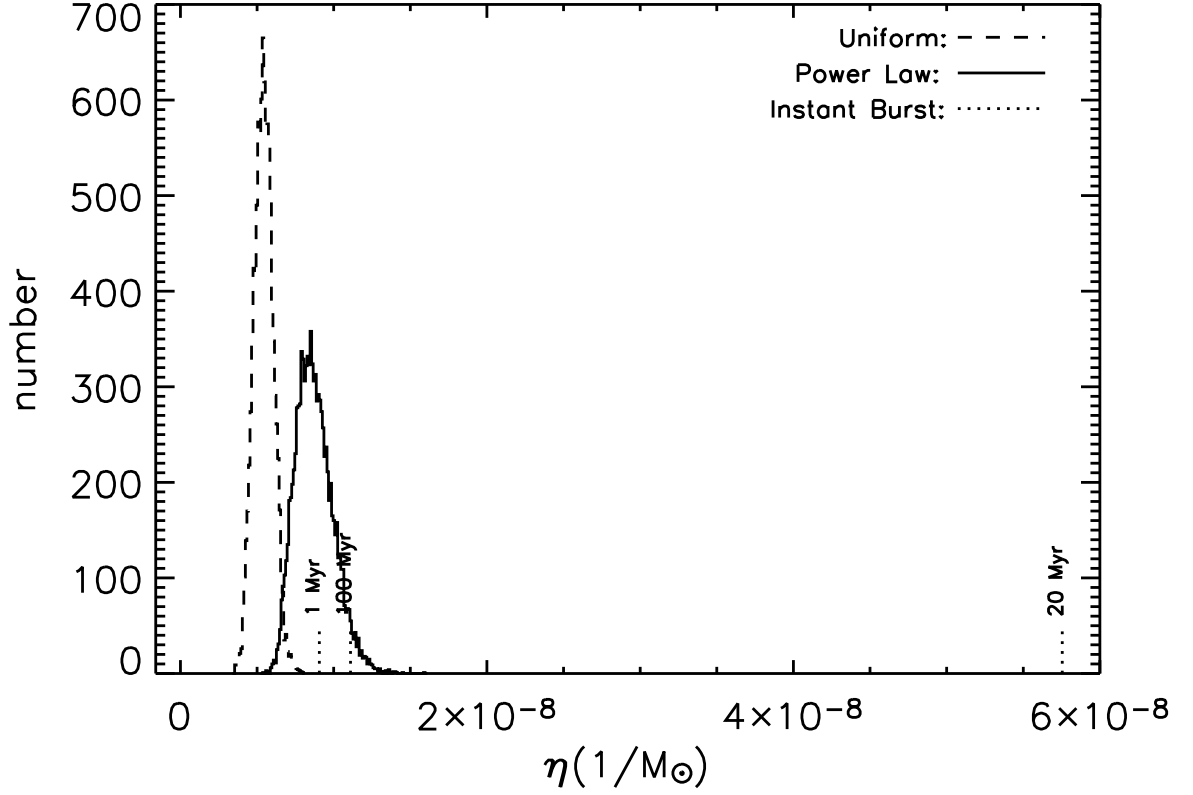


Fig. 4.— Comparison between uniform and PL Monte Carlo simulations of  $\eta$ . The peaks of each distribution vary by a factor of  $\sim 2$  in  $\eta$ , indicating  $\eta$  does not significantly change when we assume different age distributions for the Antennae. We also plot the values of  $\eta$  for instantaneous bursts at three different ages.

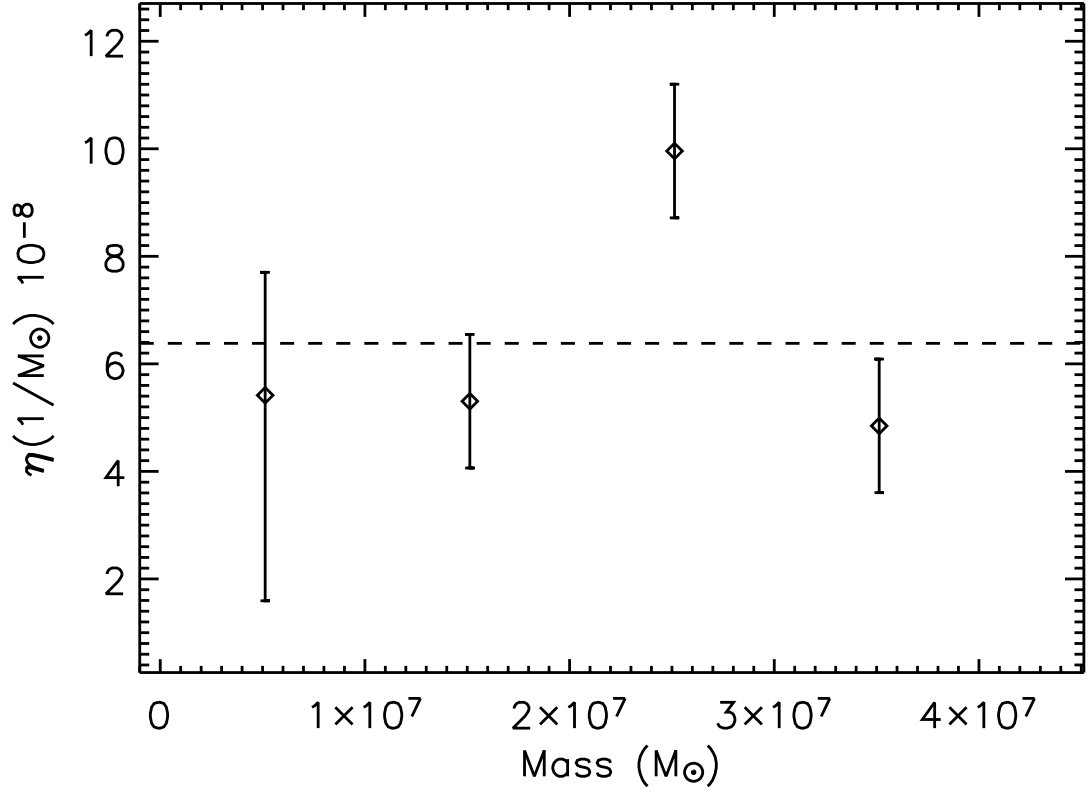


Fig. 5.— Here  $\eta$  is plotted versus cluster mass in units of  $M_{\odot}$ . In this case, we computed cluster mass using ages provided by Mengel (2005) (see §3). The bins are  $M_{\odot} = 1 \times 10^7 M_{\odot}$  in size. Error bars are the uncertainties in the mean value of  $\eta$  added in quadrature with the Poisson uncertainty in each bin. The dotted line is the mean value of the four  $\eta(M_{\odot})$ .

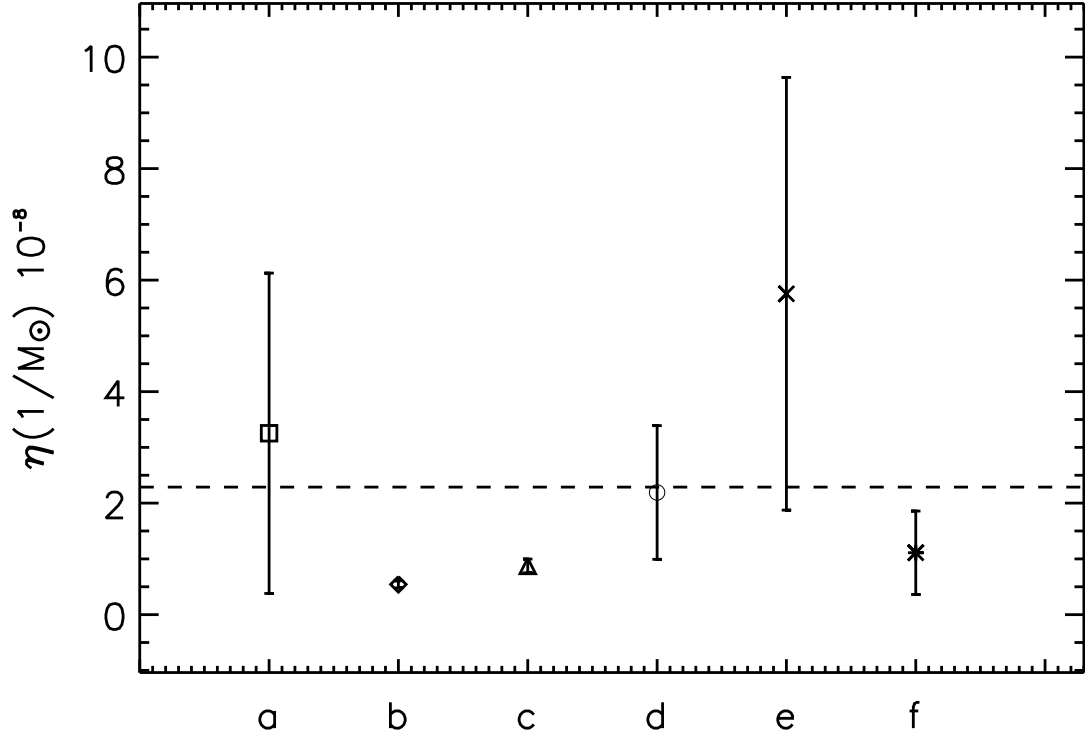


Fig. 6.— Here we summarize how age affects  $\eta$ , assuming four different age distributions for the Antennae clusters: instant burst (a), uniform (b), power law (c) and derived ages by Mengel (2005) (d). Each value is the mean  $\eta$  and includes 1- $\sigma$  error bars. See text for details. Also included is  $\eta$  for an instant starburst of 20 Myr (e) and 100 Myr (f).